Appl Phys B (2010) 101: 689–700
DOI 10.1007/s00340-010-4145-0

Applied Physics B
Lasers and Optics

NO excitation and thermal non-equilibrium within a flat plate boundary layer in an air plasma

D. Studer · P. Boubert · P. Vervisch

Received: 2 April 2010 / Revised version: 18 June 2010 / Published online: 20 July 2010

Abstract Optical emission spectroscopy experiments are carried out by recording the radiation from the γ transitions of nitrogen monoxide in an air inductively coupled plasma in interaction with a water-cooled metallic flat plate at moderate pressure. The calibrated results allow to derive the vibrational and rotational temperatures of the NO($A^2\Sigma^+$) excited state as well as its densities in the free jet and within the boundary layer by comparison with calculated spectra. Those results are compared with previous ones concerning temperatures and densities of the ground states of the majority species (N_2, O_2 and NO) that were obtained by laser techniques. As for the NO($X^2\Pi$) ground state, vibration and rotation of the excited state are found out of equilibrium. The NO($A^2\Sigma^+$) excited state is found to be populated by an energy transfer from the metastable $N_2(A^3\Sigma_u^+)$. The steady state of the plasma allows using this property to derive $N_2(A^3\Sigma_u^+)$ densities and N_2 electronic excitation temperatures. Close to the wall, a production of excited NO by a catalytic process is also considered involving $N_2(A^3\Sigma_u^+)$ as source of adsorbed atoms. The present results confirm that the kinetic temperature cannot be compared to the rotational temperature derived from optical emission spectroscopy in such plasma conditions.

1 Introduction

The re-entry of a space vehicle in the atmosphere of Earth benefits from a 50-year experience, from the first manned orbital missions to the space shuttle flights, and in particular from the Apollo missions coming back from the Moon. Reusable materials were developed that ensure a safe re-entry for velocity smaller than 8 km/s. For larger velocities, ablative materials as those used for the solar system exploration missions are preferred. The projected sample return missions and eventually manned missions to Mars will require large entry velocities (up to 15 km/s) in the Martian atmosphere as well as in the Earth atmosphere in order to limit the journey duration. Such high velocities challenge the actual knowledge in non-equilibrium plasma physico-chemistry especially concerning non-equilibrium radiative fluxes, radiative ablation products and catalycity of materials.

The existing physical and chemical models met some success in predicting ground state densities including in non-equilibrium conditions, but failed to deal with excited species [1, 2]. Vibrational specific [3, 4] or electronic specific [5] collisional-radiative models that are in development are expected to bring the needed answers. Nevertheless, some test cases are necessary to validate such models, and the purpose is to fully characterize some plasmas in interaction with thermal protection system (TPS) materials [6]. This means measuring ground state densities as well as excited states' densities and determining the energy distribution in internal modes or temperatures when they are suitable. Temperatures are indeed one of the easiest data to obtain especially through optical diagnostic techniques. Optical emission spectroscopy (OES) is a powerful tool to get those temperatures when equilibrium is ensured between ground state energy modes and excited state energy modes [7–9]. However, some assumptions about equilibrium between energy storage modes should be made very carefully in some non-equilibrium plasmas. Nevertheless, OES is often used as a temperature diagnostic method in in-

D. Studer · P. Boubert (✉) · P. Vervisch
CORIA—UMR 6614 CNRS, Université et INSA de Rouen,
76801 Saint-Etienne du Rouvray Cedex, France
e-mail: boubert@coria.fr

ductively coupled plasmas [10–14] as well as in arc-jets [15, 16]. The usual assumptions about the equilibrium between rotation and translation, or between vibration and electronic excitation and/or electron should take into account the ways internal modes are populated, and they depend on the pressure, the surface interactions, the plasma production process, the electron density, the kinetic temperature, etc. A limitation of the thermal description of those non-equilibrium plasmas to a strict two-temperature model may lead to significant errors.

On the other hand, the characterization of the plasma cannot be limited to the knowledge of ground state behaviors because many critical processes during an atmospheric re-entry involve excited particles and especially metastable particles. At high entry velocities in air, the radiative energy term becomes as important as the convective energy term. The transfer of that energy to the spacecraft wall is a key issue [17]. Many experimental studies were conducted on air plasma in the frame of atmospheric entry activities or for other purposes. The difficulty is often to gather all the diagnostic techniques that are necessary to track most of the majority species of the plasma. Desportes [18] studied an air plasma flow in the same facility as described below but with a quite higher specific enthalpy, and detected emission from atomic oxygen and nitrogen as well as from molecules: N_2 first and second positive systems, N_2^+ first negative systems and ϵ and γ bands of NO. The aim of this paper is to complete the characterization of a moderate pressure non-equilibrium plasma expected to reproduce atmospheric entry shock layer conditions. It is a prospective study concerning the issue of interaction of plasmas with TPS materials and the role of catalycity. After a description of the facility and experimental set-up and after recalling the main results of previous studies about ground state species [19, 20], we focus on the results of NO emission spectroscopy concerning temperatures and densities. Those data are then analyzed together with previous ground state results to feed a discussion about the excitation processes in the plasma and about non-equilibrium between the energy storage modes.

2 Plasma wind tunnel

The experiments were carried out in the CORIA research center 100 kW inductively coupled plasma wind tunnel. The plasma generator is made of a quartz tube whose internal/external diameters are 72/80 mm surrounded by five RF water-cooled coils. The 1.7 MHz oscillations are ensured by a triode. The gas injection is mainly (95%) annular and weakly swirled (10°). The plasma is conventionally ignited with argon then switched to synthetic air (80% nitrogen and 20% oxygen). A weak amount of air (5%) is injected axially to maintain the plasma between coils. The

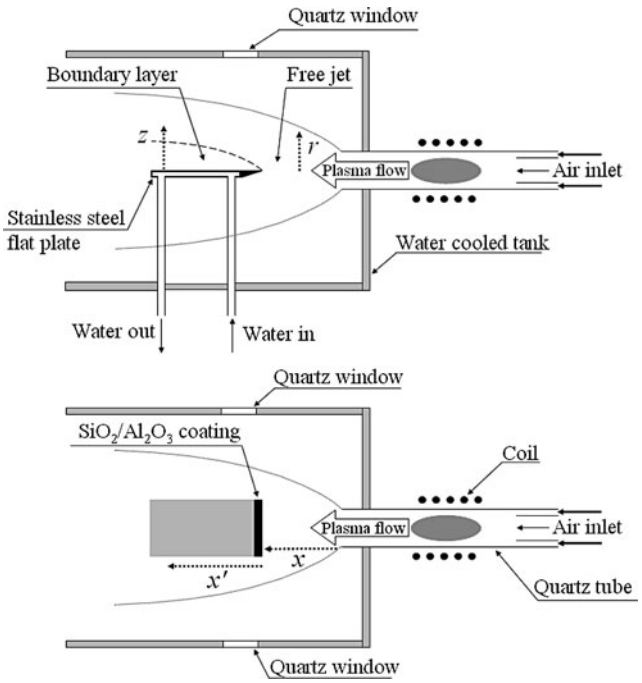

Fig. 1 Free jet, boundary layer and coordinate system

plasma expands in a cylindrical test chamber (0.5 m in diameter). It is water-cooled and equipped with three optical access ports around, that are movable even when the pressure in the chamber is low. During this campaign, the power sent to the inductor was 42 kW and the mass flow rate was fixed to 2.4 g/s. Considering an efficiency coupling estimated at 50 $\pm$ 10%, those values correspond to a specific enthalpy close to 9 MJ/kg and a plasma jet velocity equal to 250 m/s (so clearly subsonic in these conditions). The measurements were performed both in the plasma free jet and over a metallic flat plate. That plate was made of stainless steel and cooled down to 300 K by a water circulation. It was 100 mm wide and 150 mm long. The leading edge was coated with mullite (Al_2O_3/SiO_2) 5 mm long layer to prevent it from oxidation by atomic oxygen. The leading edge was located 80 mm downstream from the quartz tube exit. Concerning results obtained in the free jet, the distance from the quartz tube is called x while the radial location is r. Within the boundary layer over the flat plate, the distance from the leading edge is called x' while the distance over the plate is z. This coordinate system is shown in Fig. 1 with an overview of the experimental set-up.

3 Results about ground states

Previous studies used laser diagnostics such as spontaneous Raman scattering (SRS) [19] and laser-induced fluorescence (LIF) [20] to track ground state densities and temperatures

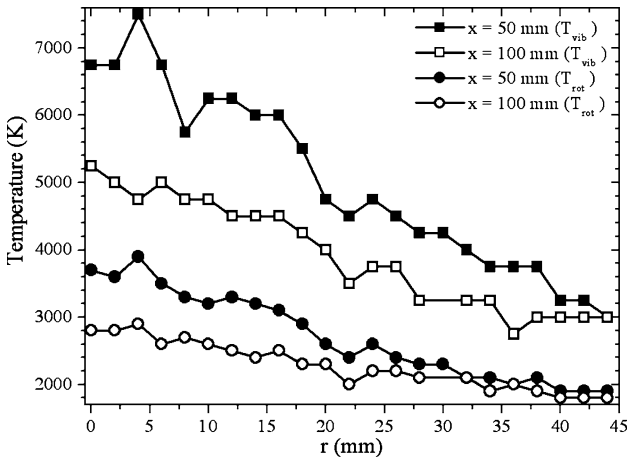

Fig. 2 Profiles of the NO($X^2\Pi$) vibrational and rotational temperatures in the free jet

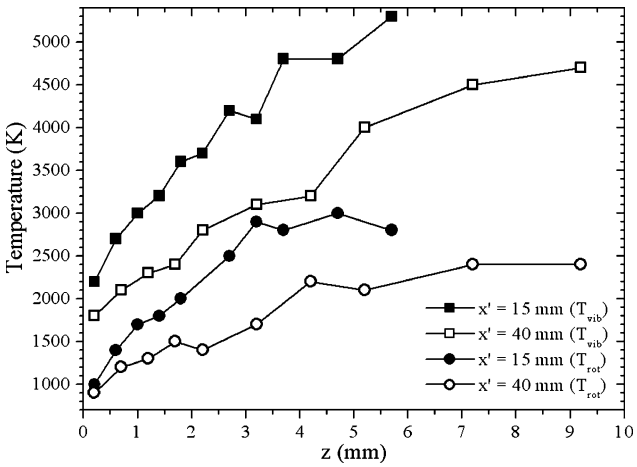

Fig. 3 Profiles of the $N_2(X^1\Sigma^+)$ vibrational and rotational temperatures within the boundary layer

of majority species, i.e., N_2, O_2 (Raman) and NO (LIF), both in the free jet and within the boundary layer.

In the free jet, no measurement was possible on O_2 because of its too high dissociation rate. SRS measurements on N_2 led to quite constant rotational (2500 K) and vibrational (5200 K) temperatures whatever the section in the first 100 mm from the quartz tube exit. For NO, some LIF measurements underlined the non-equilibrium between rotation and vibration and also showed that the corresponding temperatures decreased along the jet axis (Fig. 2). The NO vibrational temperature was found to be different from the N_2 and O_2 vibrational temperatures. The conclusion was that a vibrational excitation for each species should be considered in numerical multi-temperature simulations.

Within the boundary layer, the non-equilibrium between vibration and rotation remains whatever the molecules in spite of different spatial evolutions (Figs. 3 to 5). A rather good accommodation of the rotational temperature on the wall is measured especially for N_2 and O_2. Conversely, although the vibrational temperature decreases from the jet to the wall, it does not reach the wall temperature and remains high, especially for NO. Moreover, LIF measurements revealed a non-equilibrium production of NO close to the wall through Zel'dovich mechanisms, i.e., atom exchanges between molecules and atoms.

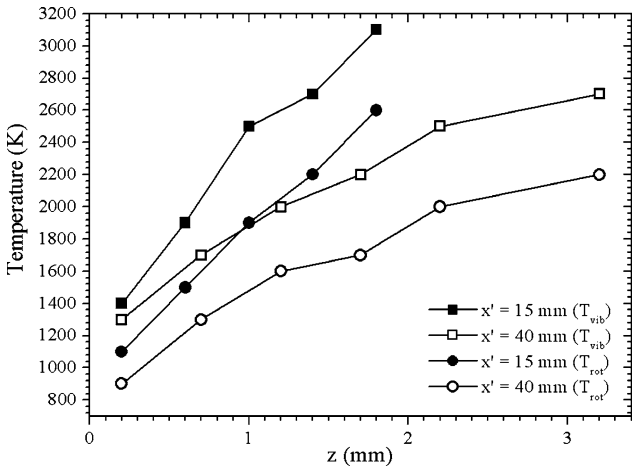

Fig. 4 Profiles of the $O_2(X^3\Sigma^+)$ vibrational and rotational temperatures within the boundary layer

4 Optical emission spectroscopy

4.1 Optical set-up and calibration

The spontaneous emission of the plasma was collected by a single fused-silica lens and analyzed using a spectrometer Jobin-Yvon THR1000 equipped with a UV grating (4320 gr/mm) providing a sufficient spectral resolution for rotational temperature determinations. The resulting spectral spatial image was then recorded on an intensified charge-coupled device (ICCD) camera Princeton Instruments PI-MAX optimized for UV measurements. The spectrometer used was not designed for flat field acquisitions but some tests showed that the expected image distortions were negligible. In order to carry out an Abel inversion on the measurements performed in the axisymmetrical free jet, it was necessary to collect light from at least one jet radius from the center to the external border. The spectrometer entry slit was opened vertically to 10 mm. The lens focal length was 89 mm at 230 nm. The lens was set in order to get a magnification ratio equal to 0.14. In those conditions, the measurement field was 72 mm in height and the spatial resolution along the plasmas axis was 0.28 mm. The spectral resolution was mainly limited by the CCD element effective size (24 μm). In the free jet, the observed spectral resolution was 0.027 nm.

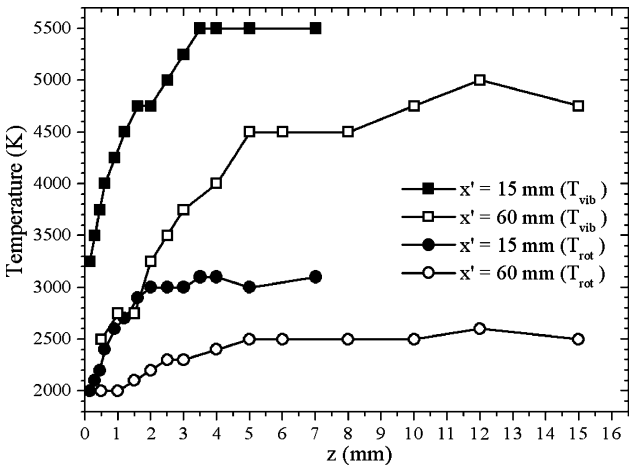

Fig. 5 Profiles of the NO($X^2\Pi$) vibrational and rotational temperatures within the boundary layer

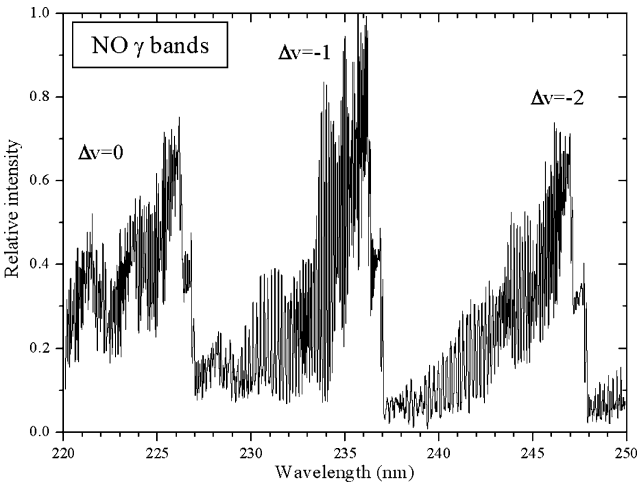

Fig. 6 NO γ emission spectrum between 220 and 250 nm

The optical set-up was different for measurements within the boundary layer. That led to a slightly better spectral resolution estimated to 0.025 nm. For those measurements, the set-up consisted of a single fused-silica lens with a focal length equal to 200 mm at 230 nm. The corresponding magnification ratio was 0.34 that allows capturing 25 mm above the flat plate. This field height was sufficient to analyze the whole boundary layer even 70 mm from the leading edge. The spatial resolution along the plasma axis was then 0.68 mm.

The measured intensities are converted to absolute intensities by calibrating the optical setup using a calibrated deuterium lamp. Considering the intrinsic uncertainty on the deuterium lamp intensity and our measurement process, the error on the calibration is low and close to $\pm 5\%$.

4.2 Determination of temperatures and densities

The spontaneous emission spectrum of NO along the γ transitions was observed between 220 and 250 nm, corresponding to the vibrational manifolds $\Delta v = 0, -1$ and -2. Those bands correspond to the rovibronic de-excitation from the $A^2\Sigma^+$ excited state to the $X^2\Pi$ ground state. A typical spectrum of NO γ bands is show in Fig. 6 with the manifold assignment.

In order to get local data, the radial emission profiles were Abel inversed. This is a well known procedure in an axisymmetrical emitting medium. Conversely, local data cannot be derived from the profile obtained within the boundary layer without assumptions. The emission profiles were shown to be identical outside the boundary layer and at the same location in the free jet. Moreover, most of the emitted light was expected to come from the hottest part of the plasma (i.e., on the axis), and cold border emission does not disturb the measured profiles. Last, the plate was thin enough not to cause significant edge effects. According to those arguments, we supposed that the spatial profile shapes along the light collection axis were not modified by the flat plate. So Abel inversed profiles within the boundary layer were sought with a similar shape as in the free jet at the same location.

We derived densities and temperatures by comparing the calculated spectra and Abel inversed spectra. The procedure was to derive rotational and vibrational temperatures from normalized spectra then to estimate the excited state density by comparing the absolute calculated and absolute experimental spectra. In order to obtain some calibrated experimental spectra, the irradiance of a calibrated deuterium lamp was recorded with the same optical set-ups as for emission measurements in the free jet and within the boundary layer.

We carried out the calculation of spectra by determining the ground and excited state rovibronic energy levels according to spectroscopic data published by Amiot [21] for the $X^2\Pi$ ground state and Danielak et al. [22] for the $A^2\Sigma^+$ excited state. Some attempts were done to model the kinetic momentum coupling transition occurring for a rotational quantum number close to 8.5 on the ground state. However, in spite of a notable modification of the intensity of the first sub-branch bandhead at 237 nm, the best agreement with experimental spectra was obtained with a Hund case (b) model (low coupling of the electron-spin angular momentum, on the one hand, and the electron-orbital angular momentum and nuclear-rotation angular momentum, on the other hand). The rotational transition probabilities were calculated according to Kovács [23], and some experimental accurate vibrational transition probabilities were given by Luque and Crosley [24].

After having determined the rotational and vibrational temperatures, on the one hand, and the excited state density, on the other hand, by a least-squares method, the uncertainties were estimated by calculating the residue; the residue

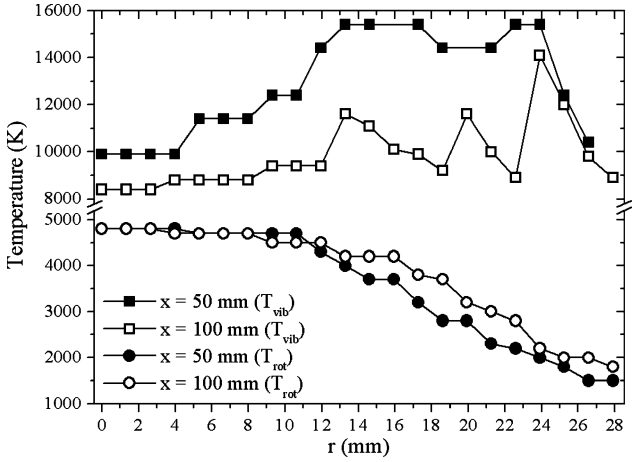

Fig. 7 Radial profiles of the NO($A^2\Sigma^+$) vibrational and rotational temperatures in the free jet

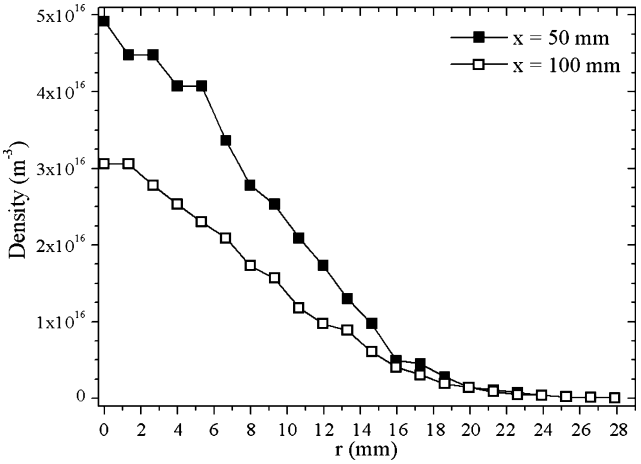

Fig. 8 Radial profiles of the NO($A^2\Sigma^+$) density in the free jet

being

$$N(T_j) = \sum_{\lambda_i} \left[I_{\text{exp}}(\lambda_i) - I_{\text{calc}}^{T_j}(\lambda_i) \right]^2$$

with T_j the searched parameter. In the free jet, the uncertainty on vibrational temperatures is ±500 K for radii lower than 10 mm and ±1000 K for higher radii. The uncertainty on rotational temperatures is ±100 K for radii lower than 10 mm and ±200 K for higher radii. The relative uncertainty on excited state density is about ±25%. Within the boundary layer, the uncertainties on vibrational and rotational temperatures were found to be ±500 K and ±100 K, respectively, whatever the distance to the plate and whatever the probed section. Considering the previous uncertainties, the excited state densities are known to within less than 25%. However, those uncertainties do not take into account the error on spectroscopic constants and transition probabilities. For the most populated levels, the uncertainty on the energy values is low. It increases for levels whose population is very low so that the uncertainty on the partition functions due to the spectroscopic constants is negligible. The uncertainty due to the temperatures is included. Concerning the Einstein coefficients, the uncertainty is close to 3% [24] for the measured bands. The values given by Luque and Crosley were considered to be the best available at that time.

4.3 Free jet results

We explored three sections in the free jet. They are located at 25, 50 and 100 mm from the exit of the quartz tube. Figure 7 presents the vibrational and rotational temperature radial profiles for two of these sections. The vibrational temperature is quite constant in the first ten millimetres whatever the section, but increases to very high values in the outside part of the free jet. The decrease close to 25 mm corresponds to the interaction of the jet with the outside still gas. There is a quite wide dispersion in vibrational temperature measurements due to a limited accuracy mentioned in Sect. 4.2. That dispersion increases with the distance from the axis and is especially strong when the plasma jet is mixed with the steady gas in the wind tunnel. Some aerodynamic structures are then observed, and the vibrational excitation is very sensitive to them. Conversely, the rotational temperature remains coupled to the translation temperature. Rotational temperature measurements are much more accurate and coherent. The rotational temperature is clearly constant in the center of the jet as far as 8 mm whatever the section. The values are then slightly lower than 5000 K and weakly decrease with the distance to the tube exit. The rotational temperature plots also show how the jet get wider with the distance to the tube exit since, for radii larger than 10 mm, the rotational temperature is slightly higher for $x = 100$ mm than for $x = 50$ mm. Nevertheless, the rotational temperature can be considered as homogeneous on the axis in the first 100 mm from the tube exit. Conversely, there are some differences on the density profiles as shown in Fig. 8. Of course, those values are dependent on the temperatures and the low accuracy on vibrational temperature determination has got an influence on density results.

As for the measurements concerning ground states carried out by Raman scattering and LIF (see Sect. 3), we find a strong thermal non-equilibrium between vibration and rotation.

4.4 Boundary layer results

Within the boundary layer above the flat plate, six sections were explored located at 4, 8, 18, 25, 41, and 61 mm from the leading edge. Figure 9 shows the profiles of vibrational and rotational temperatures above the flat plate for three of these sections. As for the free jet, the dispersion for the

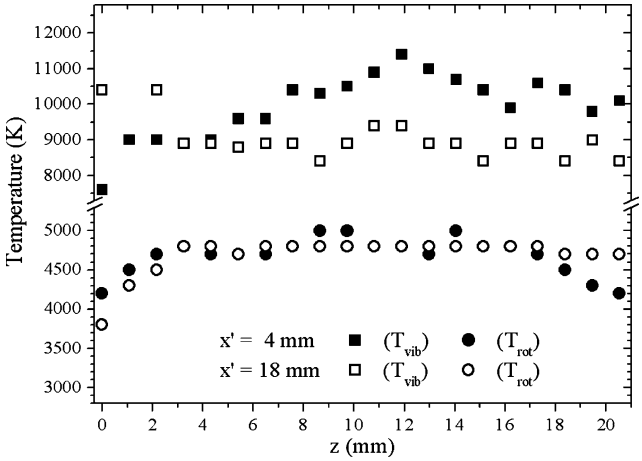

Fig. 9 Profiles of the NO($A^2\Sigma^+$) vibrational and rotational temperatures within the boundary layer

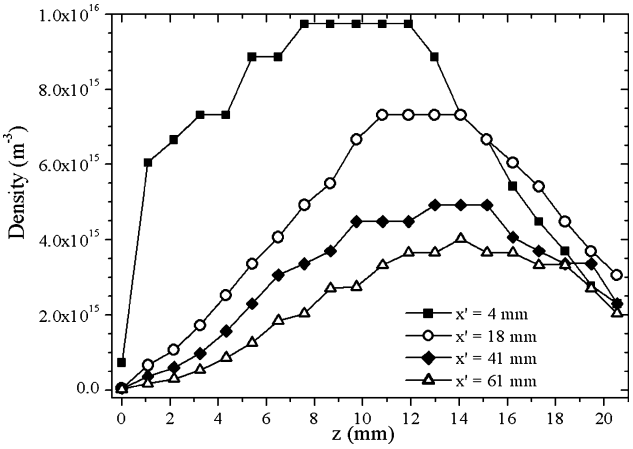

Fig. 10 Profiles of the NO($A^2\Sigma^+$) density within the boundary layer

vibrational temperature measurements is large. That temperature can be considered as constant within the boundary layer and no significant decrease is observed close to the wall. Conversely, the rotational temperature clearly decreases from the boundary layer, where the temperature is constant close to 4800 K, towards the wall. The further the section from the leading edge, the lower the rotational temperature at the wall: from 4200 K for $x' = 4$ mm to 3200 K for $x' = 41$ mm (the same value was found for $x' = 61$ mm). That better accommodation of the rotational temperature to the wall was also observed for ground state temperature of N_2, O_2 and NO measured by Raman scattering and LIF (see Sect. 3). It could be surprising to observe a constant rotational temperature above the plate where that temperature decreased in the case of the free jet. However, it should be noticed that, first, in order to encounter hottest conditions, the plate was placed 5 mm below the jet axis, and secondly, the plate made the jet veer vertically and get wider. The density profiles in the boundary layer are very interesting (Fig. 10). There is a general increase of NO($A^2\Sigma^+$) density from the wall to the boundary layer limit, then a decrease outside. It should be noticed that the density value outside the boundary layer is quite the same whatever the section. The boundary layer limit is characterized by a maximum for the density then a plateau whose length decrease with the distance to the leading edge. The maximum density in the boundary remains lower than in the free jet mainly because of a temperature effect. Another observation is the difference in the boundary layer thickness for excited NO and ground state NO: it is equal to about 12 mm for the section $x' = 18$ mm in Fig. 9, while it was only a few millimeters for NO ground state [20] as well as for N_2 and O_2 ground states [19]. A second difference is the behavior of excited NO at the wall. While the NO ground state density increases close to the wall because of Zel'dovich reactions, the NO($A^2\Sigma^+$) density clearly drops to zero. However, it will be demonstrated in the forthcoming discussion that NO is nevertheless produced on that electronic state close to the wall.

5 Discussion

NO($X^2\Pi$) ground state densities were measured by laser-induced fluorescence [20], and NO($A^2\Sigma^+$) excited state densities were measured by optical emission spectroscopy in the free jet and within the boundary layer above the flat metallic plate. Assuming that both electronic states are in Boltzmann equilibrium with each other, some electronic excitation temperatures may be calculated from the measured densities. In that case, the electronic excitation temperature T_{exc} is calculated after the ratio of upper and lower populations according to a Boltzmann distribution:

$$\frac{n^*}{n^0} = \frac{g^*}{g^0} \exp\left(-\frac{E}{k_B T_{\text{exc}}}\right)$$

with g^* and g^0 being the density of upper and lower electronic level, respectively, g^* and g^0 being their statistical weight and E the difference of energy between both. k_B is the Boltzmann constant. Those electronic excitation temperatures are plotted in Fig. 11 for the free jet together with the vibrational temperatures of NO ground state measured using laser-induced fluorescence [20]. Both temperatures are found to be close and can be considered as equal within the uncertainty. As a supplementary illustration, Figs. 12 and 13 present the comparison between the measured NO($A^2\Sigma^+$) densities in the free jet for $x = 50$ mm and $x = 100$ mm and the densities calculated from the measured NO ground state densities and considering that the electronic excitation temperature is equal to the ground state rotational temperature. In the free jet, the electronic excitation mode is clearly out of equilibrium with the NO ground

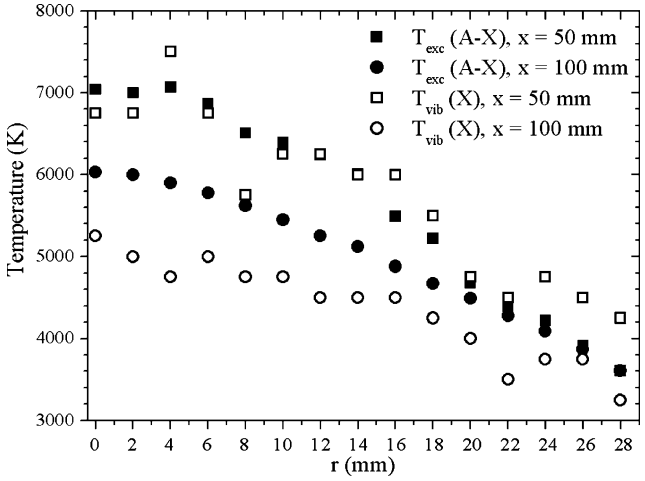

Fig. 11 Radial profiles of the NO electronic excitation temperature and ground state vibrational temperature in the free jet

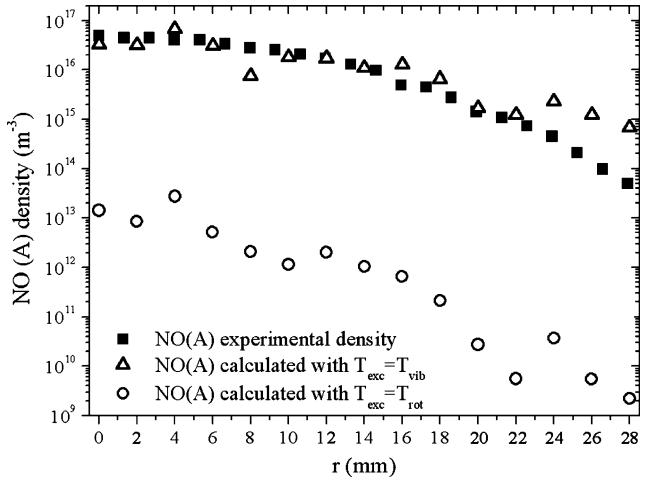

Fig. 12 Comparison between the measured and calculated NO($A^2\Sigma^+$) densities in the free jet for $x = 50$ mm; the calculation is performed from measured ground state density and both ground state vibrational and rotational temperature

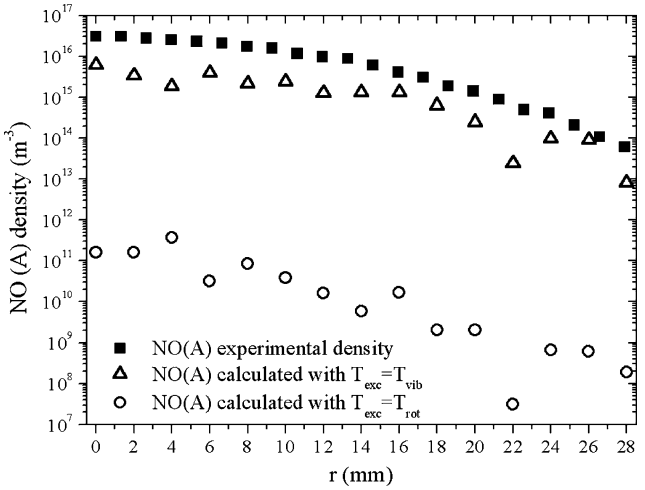

Fig. 13 Comparison between the measured and calculated NO($A^2\Sigma^+$) densities in the free jet for $x = 100$ mm; the calculation is performed from measured ground state density and both ground state vibrational and rotational temperature

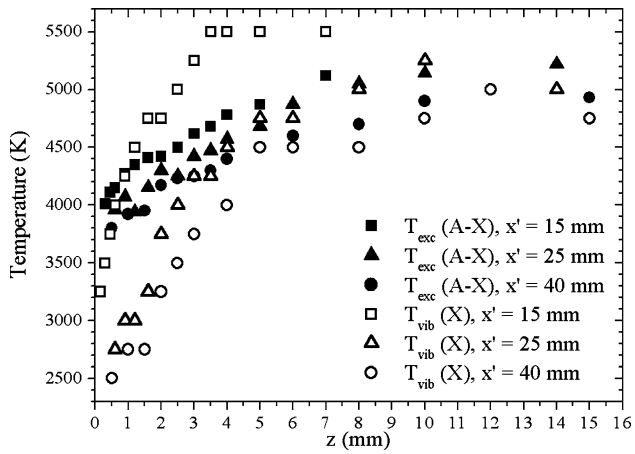

Fig. 14 Profiles of the NO electronic excitation temperature and ground state vibrational temperature within the boundary layer

state rotational mode but close to equilibrium with the NO ground state vibrational mode. It should be noticed that the NO vibrational temperatures were shown to be different to the N_2 and O_2 vibrational temperatures in the free jet [20]. In the same way, some electronic excitation temperatures may be calculated within the boundary layer. They are plotted in Fig. 14 for three sections together with the NO ground state vibrational temperatures. As expected, both temperatures are closed far from the plate, i.e., outside the boundary layer. The NO ground state vibrational temperature clearly decreases towards the wall even if vibration remains out of equilibrium with rotation as shown in Fig. 5. The calculated electronic excitation temperature has a different behavior since its decrease is much lower with a value close to about 3900 K whatever the section. At the wall, the vibrational temperature is about 2500 K and the rotational temperature about 1900 K. NO ground state density measurements underlined the production of NO molecules close to the wall through catalytic reactions, on the one hand, and in the boundary layer through Zel'dovich reactions, on the other hand [20]. Considering those last arguments, it should be suggested that NO is not only produced on its ground state but also directly on the excited electronic state $A^2\Sigma^+$ or by an excitation process that is not in equilibrium with vibration. Quantitatively, the NO($A^2\Sigma^+$) density at the wall is four orders of magnitude higher than it would be by an electronic excitation from the ground state in equilibrium with vibration. So, within the boundary layer, a two-temperature Navier–Stokes calculation is no longer able to reproduce experiments and the population of electronic

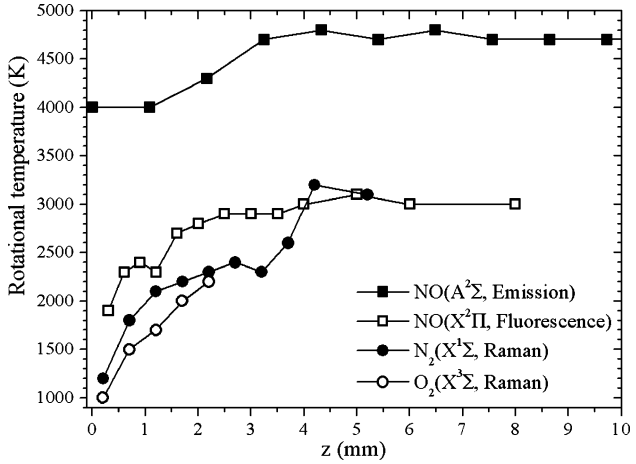

Fig. 15 Profiles of NO($A^2\Sigma^+$), NO($X^2\Pi$), $N_2(X^1\Sigma^+)$ and $O_2(X^3\Sigma^+)$ rotational temperature within the boundary layer ($x' = 25$ mm)

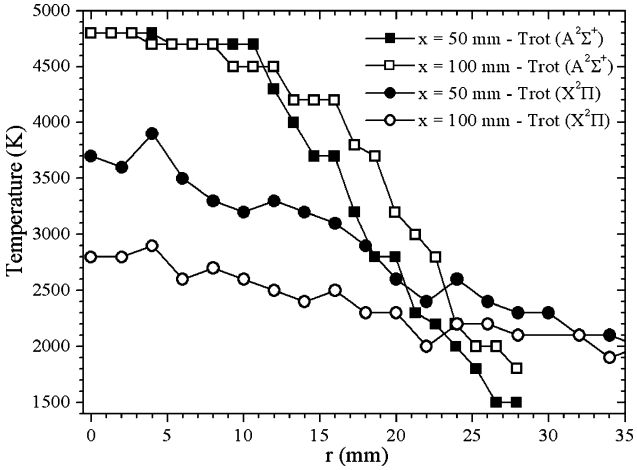

Fig. 16 Radial profiles of the NO($A^2\Sigma^+$) and NO($X^2\Pi$) rotational temperature in the free jet

excited species should be addressed through an electronic state-to-state model.

The non-equilibrium between vibration and rotation in the free jet and within the boundary layer was clearly established for the three majority species. The assumption is often made that rotation is in equilibrium with heavy particle translation. The measurements probing ground states seem to confirm that assumption especially within the boundary layer where the rotational temperature accommodates at the wall. The rotational temperatures of N_2 and O_2 ground states are very close as shown in Fig. 15. The NO ground state rotational temperature is a little bit higher (about 500 K) close to the wall but has got the same value than for N_2 at the boundary layer limit. This difference in the neighborhood of the wall could be an outcome of the exothermic chemical production of NO. Figure 15 also shows the rotational temperatures measured by emission spectroscopy on the NO($A^2\Sigma^+$) excited state. The difference between the excited state and ground state rotational temperatures is about 2000 K for a given location. This means that the rotational levels of excited molecules are not populated through a thermal excitation.

We also observed similar differences in the free jet. Figure 16 presents the radial evolution of the rotational temperature of NO on its ground and excited states for two distances from the quartz tube exit. NO ground state rotational temperatures depend on the explored section conversely to NO excited state rotational temperatures. The outcome is that the difference between both temperatures varies from 1000 to 2000 K on 50 mm along the plasma axis. The radial profiles are also very dissimilar: the excited state temperature decreases slowly and remains high even when the $A^2\Sigma^+$ state density is very low while ground state temperature quickly drops to low values.

Such a behavior of the rotational temperature of excited states was already observed in a close facility known as Comète and belonging to EADS Astrium Company [25]. Within the study on Comète, the air plasma received about 18% more power than in our experimented and its static pressure was 100 hPa. A cooled copper sample was set perpendicularly to the plasma jet. Emission measurements were carried out on molecular nitrogen ion N_2^+ and Raman scattering measurements on N_2. The rotational temperatures derived from both techniques was very different: for example, $N_2^+(B^2\Sigma^+)$ rotational temperature was equal to 7500 K while $N_2(X^1\Sigma^+)$ rotational temperature was 3500 K at 1 mm in front of the sample.

In the present study, two issues revealed by our measurements have then to be discussed: the overpopulation of NO($A^2\Sigma^+$) close to the wall and the general difference between the rotation temperatures of NO($X^2\Pi$) and NO($A^2\Sigma^+$).

In the free jet, vibrational and electronic excitation temperatures are found equal, i.e., a strong coupling may exist between the way both energy modes are excited. Some differences appear within the boundary layer and increase towards the wall. On the other hand, the difference between the rotational temperatures of NO($X^2\Pi$) and NO($A^2\Sigma^+$) has also been shown whatever the location in the plasma. We can then conclude that two processes are involved: one that is the majority in the free jet and the other that is due to the presence of the wall. Both processes produce high rotational excitation of NO($A^2\Sigma^+$).

At intermediate temperatures and reduced pressures, the main source of production of NO($A^2\Sigma^+$) was shown to be the excitation of NO ground state through a collision with a metastable species. Drakes et al. [26] showed the importance of this mechanism in low pressure combustion with

Table 1 Kinetic constants for Zel'dovich reactions [32, 33]

Reaction	A ($m^3\ s^{-1}$)	b	T_a (K)
$k_{f,(1)}$	9.45×10^{-18}	0.42	42938
$k_{f,(2)}$	4.14×10^{-21}	1.17938	4005.46

the intervention of $CO(a^3\Pi)$:

$$NO(X^2\Pi) + CO(a^3\Pi) \rightarrow NO(A^2\Sigma^+) + CO(X^1\Sigma^+). \quad (1)$$

De Benedictis et al. [27] demonstrated that $N_2(A^3\Sigma_u^+)$ is responsible for NO excitation in N_2–O_2 pulsed radio-frequency discharges:

$$NO(X^2\Pi) + N_2(A^3\Sigma_u^+) \rightarrow NO(A^2\Sigma^+) + N_2(X^1\Sigma^+). \quad (2)$$

Furthermore, Thomas and Katayama [28, 29] measured the vibrational branching ratio of both previous reactions as well as the production of $NO(B^2\Pi_r)$ but at low temperature.

In their work, De Benedictis et al. [27] also underlined the fact that the excited state rotation was not in equilibrium with translation and that no Boltzmann distribution could fit. As in the reference work by Piper et al. [30], they found a double slope Boltzmann distribution for the rotational population of $NO(A^2\Sigma^+)$ with corresponding temperatures higher than the kinetic temperature. NO excitation by metastable N_2 is assumed to preferentially populate very high rotational levels. The temperature measured by emission spectroscopy is then the effect of the rotational redistribution of this overpopulation of highly excited levels.

In the present plasma including the external part of the boundary layer, NO is produced through Zel'dovich reactions as underlined by Barbato and Bruno [31] and demonstrated in our study about NO ground state [20]:

$$N_2 + O + 3.32\ eV \rightleftharpoons NO + N, \quad (3)$$

$$O_2 + N \rightleftharpoons NO + O + 1.41\ eV. \quad (4)$$

Reaction rates of both reactions may be written as

$$k = AT^b \exp\left(-\frac{T_a}{T}\right).$$

Some constants for both forward and backward reactions are given in Table 1 for a production on the ground state. The forward reaction 3 is difficult to achieve in our conditions in spite of the large amount of N_2 and O. Conversely, the forward reaction 4 is very efficient and exothermic. Nevertheless, the energy released by this reaction is low compared to the $NO(A^2\Sigma^+)$ electronic energy, i.e., about 5 eV. Moreover, on a partially catalytic surface as a metallic plate, NO is mainly produced at the wall by catalytic reactions and especially:

$$N\ (solid) + O\ (gas) \rightleftharpoons NO\ (gas). \quad (5)$$

So we cannot affirm that the reaction 4 is able to produce a significant amount of electronically excited NO. Considering the densities, temperatures and pressure measured in the plasma, we can assume that NO excitation by metastable N_2 molecules is responsible of the observed high rotational temperatures. This is true at least in the external part of the boundary layer. Because of the steady state of the plasma, we can calculate the value of the population density of the metastable state of N_2 where this state has an exclusive role. In this case, the $NO(A^2\Sigma^+)$ production rate is equal to the de-excitation rate by quenching and spontaneous emission. That can be written as

$$k[NO(X)] \cdot [N_2(A)] = \left(Q + \frac{1}{\tau}\right)[NO(A)],$$

where k is the forward reaction rate of the reaction 2 and is taken equal to $10^{-16}\ m^{-3}\ s^{-1}$ according to Piper et al. [30]. Q is the global quenching rate and is estimated from the measured densities [19, 20] and the quenching cross-sections of $NO(A^2\Sigma^+)$ by the present species: N_2, O_2, NO [34] and O [35, 36]. τ is the radiative lifetime of $NO(A^2\Sigma^+)$ equal to the inverse of the sum of the vibronic Einstein emission coefficients provided by Luque and Crosley [24]. For example, $[N_2(A)] = 1.6 \times 10^{18}\ m^{-3}$ for $x' = 25$ mm and $z = 6$ mm. For that location along the metallic plate, the vertical profiles of N_2 ground state and N_2 metastable state densities are presented in Fig. 17 in the case where this kind of excitation is still the majority within

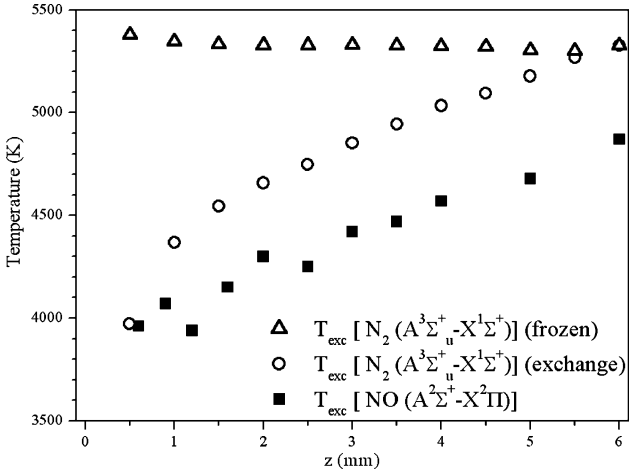

Fig. 17 Profiles of the $N_2(X^1\Sigma)$ and $N_2(A^3\Sigma_u^+)$ excitation temperature in the boundary layer for $x' = 25$ mm. Two hypotheses are considered for $N_2(A^3\Sigma_u^+)$: frozen molar fraction or responsible of NO excitation according to (2)

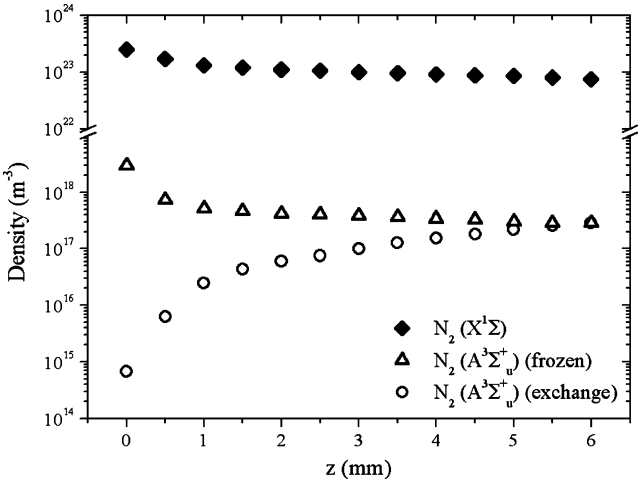

Fig. 18 Profiles of the NO($A^2\Sigma^+$–$X^2\Pi$) and $N_2(A^3\Sigma_u^+$–$X^1\Sigma)$ density in the boundary layer for $x' = 25$ mm. Two hypotheses are considered for $N_2(A^3\Sigma_u^+)$: frozen molar fraction or responsible of NO excitation according to (2)

the whole boundary layer. It shows that a production of excited NO by energy transfer from $N_2(A^3\Sigma_u^+)$ means a large decrease of this species close to the wall.

We can then calculate the electronic excitation temperature between the metastable $A^3\Sigma_u^+$ and ground $X^1\Sigma^+$ states of N_2. It is equal to 5300 K for this location. That derived temperature has to be compared to the vibrational temperature of N_2 ground state that was found equal to 5200 ± 200 K for this point (see Fig. 4 and Sect. 3). This closeness between electronic and vibrational temperature of N_2 can be found everywhere in the free jet and in the outside part of the boundary layer. Because of the indirect character of $N_2(A^3\Sigma_u^+)$ density measurements, the electronic temperature of N_2 can not be known close to the wall but as expected clearly decreases towards the wall (Fig. 18).

In fact, in the closest 6 mm, the discussion is more tricky because other processes may be involved in the NO excitation. Some of them can be dismissed as the production of excited NO by reaction of atoms with NO_2 and N_2O. The related reaction rate can be found, for example, in [37]. The thermodynamic conditions make NO_2 and N_2O minority species. The direct excitation of ground state NO by electrons is also a minority process because of the high electron recombination rate at the exit of the ICP torch and especially in the vicinity of a metallic wall. The production of NO by Zel'dovich reactions involving metastable atoms such as $O(^1D)$ can be also rejected. A simple calculation would produce unrealistic values of metastable atom densities. Moreover, no physical reason can justify higher metastable atom densities in the boundary layer compared to the free jet. Piper [38] did not mention any production of NO($A^2\Sigma^+$) in his study of the reactions:

$$N(^2D) + O_2 \rightleftharpoons NO + O, \tag{6}$$

$$N(^2P) + O_2 \rightleftharpoons NO + O. \tag{7}$$

The first forward Zel'dovich reaction 3 involving ground states is endothermic, but the activation energy can be brought by $N_2(A^3\Sigma_u^+)$ electronic excitation. Kossyi et al. gave a constant rate $k = 7 \times 10^{-18}$ m^3/s for the reaction

$$N_2(A) + O \rightleftharpoons NO + N, \tag{8}$$

where the products are NO($X^2\Pi$) and N(^{2}D). However, the remaining energy is unable to produce NO on an electronic excited state.

A third way to produce excited NO by involving metastable N_2 could be catalytic reactions at the wall. We showed in a previous study [39] that CN could be produced from a carbon surface, especially when excited N_2 molecules had previously been adsorbed. In the present case, $N_2(X^1\Sigma^+$,v) could play the role. Nevertheless, the process is efficient for high energy because of the energy involved as heat transferred to the surface, as desorption work and finally as excitation of the desorbed molecules. $N_2(A^3\Sigma_u^+)$ could provide this energy but needs a potential well on the surface since its excitation energy is lower than the dissociation energy. Its density could not exceed a few 10^{18} m^{-3} (due to the temperature effect), while the NO($A^2\Sigma^+$) is a few 10^{15} m^{-3} within the boundary layer (Fig. 10). $N_2(A^3\Sigma_u^+)$ is expected to have a low decrease in the boundary layer, but its behavior at the wall remains unknown. It is generally admitted that the metastable molecules of N_2 are able to produce Auger electrons when they encounter a cold surface. Assuming that no $N_2(A^3\Sigma_u^+)$ is created or destroyed within the boundary layer, new N_2 electronic excitation temperatures can be calculated. They are also displayed in Fig. 18 for $x' = 25$ mm and can be compared with the NO electronic excitation temperature and N_2 electronic excitation temperature in the case of a complete energy transfer from $N_2(A^3\Sigma_u^+)$.

Whatever the main excitation process of NO close to the wall, $N_2(A^3\Sigma_u^+)$ plays a major role. Moreover, emission spectroscopy (or any techniques probing exciting states) is unable to provide an estimate of the kinetic temperature in such non-equilibrium conditions. Excited-state rotational temperatures and the kinetic temperature are definitively not correlated.

6 Conclusion

A comprehensive study of a non-equilibrium air plasma in interaction with a metallic flat plate under moderate pressure (38 hPa) was carried out using optical emission spectroscopy, Raman scattering and laser-induced fluorescence. It brought the ground state temperatures and densities of majority species N_2, O_2 and NO and the temperatures and

densities of the NO($A^2\Sigma^+$) excited state. Some observations concerning non-equilibrium have to be underlined especially about nitrogen monoxide. While the vibrational and rotational NO temperatures are generally supposed to quickly equilibrate, especially in the frame of modeling, they have been found to remain very different in the free jet as well as within the boundary layer. This difference between vibrational and rotational temperatures is verified for the ground state as well as for the $A^2\Sigma^+$ excited state that is populated out of equilibrium with heavy particle translation. For most locations, an electronic excitation temperature may be identified to the vibrational temperature of the ground state $X^2\Pi$. Last, while temperatures are often determined by emission spectroscopy in plasma, the temperatures measured on the $A^2\Sigma^+$ excited state are completely different from those measured on the ground state within the boundary layer as well as in the free jet. This last point questions the way the excited state is populated from the ground state or from a chemical process. In the case of NO($A^2\Sigma^+$), the metastable state of N_2 plays a major role in energy transfers through collisions or as source of adsorbed atoms in the case of catalytic reactions. The multiple temperatures identified in the plasma also suggest paying attention to the validity of an unique rotational temperature equal to the heavy particle kinetic temperature in such moderate pressure non-equilibrium plasmas. Such an assumption is very important for radiation predictions.

This study could be extended in order to study other excited states such as $N_2(B^3\Pi_g)$, $N_2(C^3\Pi_u)$ and $N_2^+(B^2\Sigma^+)$ in order to completely characterize the plasma radiation from ultraviolet to near-infrared and to explore the formation processes of other species than NO. A knowledge of the population of the nitrogen metastable state $N_2(A^3\Sigma_u^+)$ will bring some quantitative data to support the hypothesis about the role of this state in much chemical reactions. Because of the plasma stability, it could be achieved by multipass absorption spectroscopy on the first negative system or by laser-induced fluorescence through the same system. The last important species not probed for the moment is atomic oxygen. Two-photon absorption laser-induced fluorescence seems to be the most direct way to measure its density but alternative methods such as Raman scattering based on the ground state triplet structure are possible. Up to now, attempts to measure electron temperatures and densities failed because of the oxidation of tungsten and iridium Langmuir probes. Electron density is supposed to be low but no data are available about a possible equilibrium with an energy mode of molecules and atoms.

One more next step is to resume the presently described experiments within the boundary layer of a SiC sample set perpendicularly to the plasma jet and with a higher static pressure close to 100 hPa and a higher specific enthalpy close to 20 MJ/kg. Nevertheless, the present results are already very useful to drive Navier–Stokes calculations that should take into account vibration of each kind of molecules as well as the bad accommodation of vibration to the metallic wall. Comprehensive models should also include chemical reactions involving excited states of molecules. This justifies the interest in electronic state-to-state models.

Acknowledgements This work has been supported by French research agencies (CNES and CNRS) and by the ANR programme RAYHEN.

References

1. C. Park, J. Thermophys. Heat Transf. **7**, 385 (1993)
2. C. Park, R.L. Jaffe, H. Partridge, J. Thermophys. Heat Transf. **15**, 76 (2001)
3. S.M. Chauveau, C.O. Laux, J.D. Kelley, C.H. Kruger, AIAA Paper 2002-2229 (2002)
4. S.M. Chauveau, J.D. Kelley, C.O. Laux, C.H. Kruger, AIAA Paper 2003-0137 (2003)
5. A. Bultel, B.G. Chéron, A. Bourdon, O. Motapon, I.F. Schneider, Phys. Plasmas **13**, 043502 (2006)
6. A. Kolesnikov, M.I. Yakushin, I.S. Pershin, S.A. Vasil'evskii, O. Chazot, B. Vancrayenest, J. Muylaert, in *Proceedings of the 4th European Symposium on Aerothermodynamics for Space Vehicles*. SP487 (European Space Agency, Paris, 2007), pp. 481–488
7. B. Benstaali, P. Boubert, B.G. Chéron, A. Addou, J.L. Brisset, Plasma Proc. **22**, 553 (2002)
8. M. Balat-Pichelin, J.M. Badie, R. Berjoan, P. Boubert, Chem. Phys. **291**, 181 (2003)
9. M. Balat-Pichelin, L. Bedra, O. Gerasimova, P. Boubert, Chem. Phys. **340**, 217 (2007)
10. A.M. Gomes, J. Bacri, J.P. Sarrette, J. Salon, J. Anal. At. Spectrom **7**, 1103 (1992)
11. C. Laux, R. Gessman, C. Kruger, R. Roux, F. Michaud, S.P. Davis, J. Quant. Spectrosc. Radiat. Transf. **68**, 473 (2001)
12. C. Laux, T. Spence, C. Kruger, R. Zare, Plasma Sources Sci. Technol. **12**, 125 (2003)
13. B. Michelt, G. Lins, R. Seeböck, J. Phys. D, Appl. Phys. **28**, 2600 (1995)
14. M. Winter, M. Auweter-Kürtz, in *Proceedings of the 3rd European Symposium on Aerothermodynamics for Space Vehicles*. SP426 (European Space Agency, Paris, 1999), pp. 429–436
15. D. Babikian, N. Gopaul, C. Park, J. Thermophys. Heat Transf. **8**, 737 (1994)
16. C. Park, M. Newfield, D. Fletcher, T. Gökçen, S. Sharma, J. Thermophys. Heat Transf. **12**, 190 (1998)
17. J.M. Lamet, Y. Babou, P. Rivière, M.Y. Perrin, A. Soufiani, J. Quant. Spectrosc. Radiat. Transf. **109**, 235 (2008)
18. A. Desportes, Développement de techniques de mesure optiques pour qualifier les installations de type plasmatron: applications à des mesures de catalycité. PhD Thesis, Rouen, France (2004)
19. D. Studer, P. Vervisch, J. Appl. Phys. **102**, 033303 (2007)
20. D. Studer, P. Boubert, P. Vervisch J. Phys. D, Appl. Phys. (2010, in press)
21. C. Amiot, J. Mol. Spectrosc. **94**, 150 (1982)
22. J. Danielak, U. Domin, R. Kępa, M. Rytel, M. Zachwieja, J. Mol. Spectrosc. **181**, 394 (1997)
23. I. Kovács, *Rotational Structure in the Spectra of Diatomic Molecules* (Hilger, London, 1969)
24. J. Luque, D.R. Crosley, J. Chem. Phys. **111**, 7405 (1999)
25. B. van Ootegem, D. Conte, P. Tran, P. Vervisch, D. Studer, P. Régnier, C. Crespos, P. Larregaray, J.C. Rayez, L. Martin, in *Proceedings of the 5th European Workshop on Thermal Protection Systems and Hot Structures* SP631 (European Space Agency, Paris, 2007)

26. J.A. Drakes, W.K. McGregor, M.A. Nelius, AIAA Paper 1996-1880 (1996)
27. S. De Benedictis, G. Dilecce, M. Simek, J. Phys. D, Appl. Phys. **30**, 2887 (1997)
28. J.M. Thomas, D.H. Katayama, Chem. Phys. Lett. **214**, 250 (1993)
29. J.M. Thomas, D.H. Katayama, Chem. Phys. Lett. **241**, 583 (1995)
30. L.G. Piper, L.M. Cowles, W.T. Rawlins, J. Chem. Phys. **85**, 3369 (1986)
31. M. Barbato, C. Bruno, in *Molecular Physics and Hypersonics Flows*, ed. by M. Capitelli. NATO ASI Series C, vol. 482 (1996), pp. 139–160
32. D. Bose, G.V. Candler, J. Chem. Phys. **104**, 2825 (1996)
33. D. Bose, G.V. Candler, J. Chem. Phys. **107**, 6136 (1997)
34. T.B. Settersten, B.D. Patterson, J.A. Gray, J. Chem. Phys. **124**, 234308 (2006)
35. P.H. Paul, C.D. Carter, J.A. Gray, J.L. Durant, J.W. Thoman, M.R. Furlanetto, Correlations for the NO $A^2\Sigma^+$ ($v' = 0$) electronic quenching cross section. Technical report, Sandia National Laboratories, Livermore CA, USA (1995)
36. J.A. Gray, Private communication (2008)
37. I.A. Kossyi, A.Yu. Kostinsky, A.A. Matveyev, V.P. Silakov, Plasma Sources Sci. Technol. **1**, 207 (1992)
38. L.G. Piper, J. Chem. Phys. **98**, 8560 (1993)
39. P. Boubert, P. Vervisch, J. Chem. Phys. **112**, 10482 (2000)